IEEE Access
Multidisciplinary | Rapid Review | Open Access Journal

Received December 18, 2020, accepted January 4, 2021, date of publication January 8, 2021, date of current version January 13, 2021.

Digital Object Identifier 10.1109/ACCESS.2021.3049779

Numerical Analyses of the Polarization Dependent Cladding Mode Coupling in Localized Fiber Bragg Gratings

FANGCHENG SHEN[1] AND TINGTING ZHANG[2]

[1]State Key Laboratory of Precision Electronic Manufacturing Technology and Equipment, School of Electromechanical Engineering, Guangdong University of Technology, Guangzhou 510006, China
[2]Institute of Photonic and Technologies, Aston University, Birmingham B4 7ET, U.K.

Corresponding author: Tingting Zhang (zhangt16@aston.ac.uk)

This work was supported by the Natural Science Foundation of Guangdong Province, China, under Grant 2019A1515011229.

ABSTRACT The polarization dependence of cladding mode coupling in fiber Bragg grating (FBG) plays a significant role in the excitation of surface plasmon resonances (SPR) for sensing applications. In this work, we numerically analyze the polarization dependent cladding mode coupling enabled by localized fiber Bragg gratings (LFBGs), focusing on the properties that generate from the modal structures and the position of the localized refractive index modifications (RIMs). Our analyses reveal that, both centric and eccentric LFBGs allow strong coupling to cladding modes. In centric LFBGs, coupling to EH/HE$_{1,m}$ modes dominates, whereas in eccentric LFBG, additional coupling to high azimuthal order cladding modes is permitted. Strong polarization dependence is found in eccentric LFBG: for certain cladding modes, coupling from one polarization can be suppressed due to the cancellation of negative and positive mode coupling. More interestingly, we found that cladding modes with even and odd azimuthal orders response differently to input polarizations, which accounts for the unique polarization dependence (i.e., neighboring resonances exhibit opposite polarization preference in the transmission spectra) in eccentric LFBG. Our numerical results can be verified by the good agreement with existed experimental reports.

INDEX TERMS Fiber gratings, optical fiber sensors, refractive index sensing.

I. INTRODUCTION

The excitation of cladding modes in normal single mode fiber (SMF) with tilted fiber Bragg grating (TFBG) has attracted considerable attention in fiber sensing, such as sensing of torsion and especially the sensing of surround refractive index (SRI), which is a useful parameter for bio/chemical applications [1]–[6]. In TFBG, the forward propagating core mode is coupled to backward propagating core mode and cladding modes, resulting in comb-like transmission spectra. Since the cladding modes are sensitive to SRI, TFBG can be applied directly in SRI sensing through monitoring its spectrum [1]. Moreover, the coupling to cladding modes in TFBG depends strongly on the input core mode polarization. Such polarization dependence, combined with the comb-like spectrum of TFBGs, enables high resolution interrogation of TFBG based surface plasmon resonance (SPR) sensors [7].

The associate editor coordinating the review of this manuscript and approving it for publication was Muguang Wang.

Inspired by the high SRI sensing performance of TFBG, localized fiber Bragg grating (LFBG), which exhibits comb-like transmission spectra similar to that of TFBG, has attracted intensified research attention recently [8], [9]. Usually, LFBG is inscribed with femtosecond laser point by point (PbP) method, and is characterized with refractive index modulation (RIM) occupying only part of the fiber core (Fig. 1a) [10]–[12]. Compared with TFBG, LFBG can be inscribed without phase masks, enabling more flexible grating design. According to whether the RIM locates at the core center, LFBG can be classified into centric LFBG (CLFBG) and eccentric LFBG (ELFBG) [8]. Thomas *et al.* established the RIM model of LFBG and analyzed the cladding mode coupling of LFBG, focusing on the modal properties and transmission spectra of single polarization [13], [14]. Chah *et al.* successfully applied ELFBG to excite SPR for SRI sensing application, where SPR was observed for one of the input polarizations [8]. Chikh-Bled et al experimentally analyzed the behaviors of ELFBG for both polarizations at high

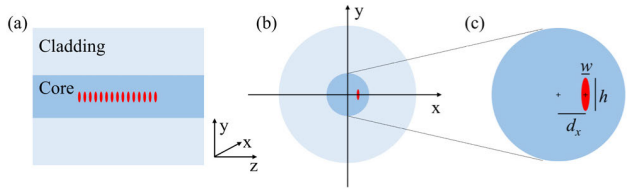

FIGURE 1. Schematic of (a) LFBG, (b) transverse RIM distribution, and (c) enlarged schematic of transverse RIM distribution within the core region, with w, h and d_x indicating the typical parameters of RIM width, height, and offset along x axis, respectively.

temperature [15], and the transmission spectra of ELFBG depend strongly on the input polarizations. As demonstrated with TFBG, polarization dependence plays a significant role in the excitation of SPR and interrogation of fiber-grating-based sensors [16]–[18]. Therefore, it will be important for the sensing application of LFBG to have detailed analyses of its polarization dependent coupling properties, which, however, are not available yet.

In this work, we adopt the RIM model laid out by Thomas but take the polarization of core mode into consideration, and present detailed numerical analyses of the polarization dependent cladding mode coupling in LFBGs, focusing on the properties that generate from the modal structures and RIM position. We show that mode cancellation is the main reason for the polarization selective coupling, and reveal the unique polarization dependence in ELFBG.

II. MODEL AND THEORY

A. MODES OF THE THREE-LAYER FIBER

In this work, a standard step-index SMF that consists of three refractive index (RI) layers (core, cladding and surrounding air, as depicted in Fig. 1a) will be considered for the mode coupling analyses. The theory of three-layer model has been well established [19], where rather complex dispersion relations are involved to calculate the effective refractive index (ERI) and mode field of each mode. For simplicity, we will not repeat those formulas and only review the notation of related modes to help understand the following work in this paper.

For normal SMF, only the fundamental $HE_{1,1}$ type mode can be guided in the fiber core, while the fiber cladding can be regarded as a multimode waveguide that supports four different types of cladding modes: $TE_{0,m}$, $TM_{0,m}$, $HE_{l,m}$, and $EH_{l,m}$. Those modes are classified according to their field distribution [13]. TE and TM modes mean transverse electric and transverse magnetic modes respectively, while HE/EH modes refer to hybrid modes. The integer l is the mode azimuthal order (AO), such that all field components have azimuthal dependence in the form of $\sin(l\phi+\varphi)$ or $\cos(l\phi+\varphi)$, and m is the mode radial order (RO) that numbers the solutions for a given l, starting from the highest ERI. The hybrid modes are degenerate between two orthogonal polarizations, referred to as even mode when $\varphi = 0$, and odd mode when $\varphi = \pi/2$. Note that for certain l, the transverse fields of even and odd mode differ by a rotation angle of $\pi/(2l)$.

B. RESONANT WAVELENGTHS

With the ERI calculated from the dispersion relation, the corresponding resonant wavelengths can be determined by the phase matching condition [20]:

$$\begin{aligned}\lambda_{co} &= 2 \cdot neff^{co} \cdot \Lambda \\ \lambda_{cl} &= (neff^{co} + neff^{cl}_{l,m}) \cdot \Lambda \end{aligned} \quad (1)$$

where λ_{co} and λ_{cl} mean the resonant wavelengths resulted from coupling to core mode and cladding mode respectively, $neff^{co}$ and $neff^{cl}_{l,m}$ represent the ERI of core and cladding mode, with (l,m) indicating the mode order, and Λ is the grating period. As the core mode has the highest ERI, its resonance can be easily identified at the longest wavelength, whereas cladding modes resonances of the same AO appear sequentially below the core mode resonance, with increasing RO from the long wavelength side.

C. COUPLING COEFFICIENTS

The interaction between modes in FBG can be described with a set of differential equations named as coupled mode equations [20], [21], where the interaction strength is determined by coupling coefficients. To calculate the coupling coefficients of LFBG, we adopt the RIM model laid out by Thomas [13]. He assumes an ellipsoidal transverse RIM distribution with a width $w = 0.4\ \mu$m and a height $h = 1.9\ \mu$m, as shown schematically in Fig. 1c, and the RIM is assumed to be uniform in the ellipse. The grating is treated as periodic rectangular modulation with a duty cycle of 50%, which can be approximated with the Fourier expansion. Based on this model, the coupling coefficients of the fundamental core mode and reflected cladding modes can be calculated with:

$$\kappa_{l,m} = \frac{4}{\pi\nu} \cdot \frac{\omega}{4} \int_0^{2\pi} d\varphi \int_0^{\infty} drr\Delta\varepsilon(r,\varphi) E_{co} E_{cl}^{l,m*} \quad (2)$$

where $4/(\pi\nu)$ accounts for the Fourier factor for LFBG with a reflection order ν, E_{co} and $E_{cl}^{l,m}$ are the transverse electric field of core mode and (l,m) cladding mode, which are calculated from the unperturbed fiber, the symbol (*) means complex conjugate, and the modulation of dielectric constant $\Delta\varepsilon(r,\varphi) = \varepsilon_0(n^2_{\text{mod}} - n_1^2)\theta(r,\varphi)$, where n_{mod} is the modulated RI, and $\theta(r,\varphi)$ describes the transverse ellipsoidal distribution of RIM, with $\theta(r,\varphi) = 1$ in the ellipse and $\theta(r,\varphi) = 0$ elsewhere. Solving the coupled mode equations with the computed coupling coefficients, we can get the transmission spectra of LFBG.

III. RESULTS AND DISCUSSION

In our calculation, the following parameters are adopted: fiber core and cladding radius are 4.1 μm and 62.5 μm respectively, the RIs of fiber core and cladding are given by the Sellmeier equation, where 3.5m% GeO_2 composition is set for core and pure silica for cladding, and the SRI n3 = 1, corresponding to the RI of air. The dispersion relation for the calculation of mode ERI [19] is transcendental and is numerically solved with Newton's method. First order CLFBG and

ELFBG with a typical 1.5 μm offset [8], [9], [22] in the x coordinate (Fig. 1c) are analyzed to investigate the effect of eccentricity on their polarization dependence. The grating period is set to give a core mode resonance at 1.55 μm, and the RIM has a value of 1.05×10^{-2}, which is achievable with femtosecond laser inscription [23]. Note that, since the fabrication process of LFBG with the femtosecond laser PbP technique is sensitive to calibration parameters, the simulation parameters in this model, such as the width and height of the RIM distribution, should be modified accordingly for a real application.

A. COUPLING COEFFICIENTS

The coupling coefficients calculated at 1.55 μm wavelength for CLFBG are shown in Fig. 2, where cladding modes with AO up to 5 and coupling from both polarizations are considered (x and y polarizations are along the x and y axis in Fig. 1b). It can be observed from Fig. 2 that coupling to HE/EH$_{1,m}$ modes dominates, and coupling to HE/EH$_{3,m}$ modes ranks the second, whereas no coupling occurs for cladding modes with even AO. Moreover, all cladding modes allow coupling from both polarizations with comparable efficiency, suggesting a weak polarization dependence.

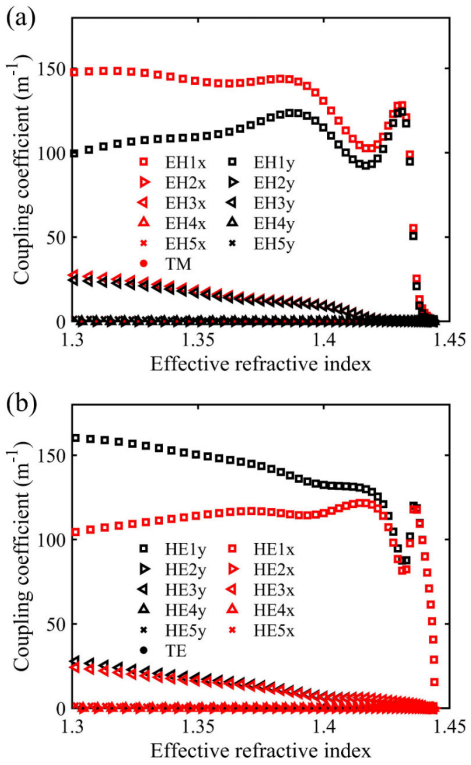

FIGURE 2. Coupling coefficients of cladding modes with AO up to 5 in CLFBG. X and y indicate the polarization along x and y axis, and are represented by red and black color, respectively.

Since the magnitude of coupling strength depends on the overlap between core and cladding mode electric field [(2)], several exemplary overlap fields for both polarizations are depicted in Fig. 3 to help understand the coupling behaviors. Since the coupling coefficients are calculated from integration over the RIM area [(2)], strong coupling is expected when the RIM occupies more area with the same and deep color. In Fig. 3, overlap fields of HE$_{l,m}$ modes are depicted only because EH$_{l,m}$ modes operate approximately the opposite way [24], as can be seen from Fig. 2. The overlap fields are calculated over the core region because the induced RIM is usually confined within the core. As can be observed from Fig. 3, the HE$_{1,10}$ cladding mode has a circularly quasi-symmetric overlap with core mode for both polarizations, with the maximum in the core center. In this case, a very weak polarization dependence is expected, no matter where the RIM locates. With the increase of mode RO (corresponding to the decrease of mode ERI), the circular symmetry of the overlap field is broken and the overlap field exhibits an ellipsoidal distribution around the core center (HE$_{1,20}$ mode in Fig. 3). For HE$_{1,20}$(y) in Fig. 3, the major axes of both ellipses (ellipse of the red area and ellipse of the RIM) are in the same direction, thus occupying more deep red area than HE$_{1,20}$(x). Therefore, the coupling from y polarization is stronger than x polarization for HE$_{1,20}$ mode (this trend can also be seen from Fig. 2b). For cladding modes with even AO, as represented by HE$_{2,20}$ mode in Fig. 3, the RIM of CLFBG locates exactly at the symmetry axis of the overlap field, as a result, the integral in (2) cancels out over the RIM region and gives a zero coupling coefficient. The coupling to cladding modes with odd AO $l > 1$ (HE$_{3,20}$ in Fig. 3), though not cancels out, is relatively weak, because the overlap field around the core center is not strong enough to support efficient coupling for those modes.

It is clear from (2) that the coupling coefficient is related to the integral domain, which is the RIM region here, so when the RIM is offset from the core center, different coupling coefficients are expected. Fig. 4 depicts the coupling coefficients of ELFBG with 1.5 μm offset along x axis. Compared with CLFBG (Fig. 2), the coupling to TE modes, TM modes, and HE/EH$_{l,m}$ modes with AO $l > 1$ is significantly enhanced, whereas the coupling to EH/HE$_{1,m}$ cladding modes become relatively weak, since the RIM is away from the core center where their overlap fields have a maximum. More of our concern is that, with the offset, polarization dependent coupling characteristics can be observed in Fig. 4. It can be seen that, in ELFBG, TE (TM) modes allow coupling from y (x) polarization only [14], [24]. For hybrid modes, to illustrate their polarization dependence more clearly, we take HE/EH$_{1,m}$ and HE/EH$_{2,m}$ modes as representative examples for modes with odd and even AO. Their coupling coefficients are depicted in Fig. 5a and Fig. 5b, respectively. We can see from Fig. 5 that the polarization dependence changes with the decrease of ERI. The initial several modes present weak polarization dependence (yellow area in Fig. 5), whereas the remaining modes show much stronger polarization preference. The polarization preference switches at ERI indicated by green arrows, i.e., from x polarization preference to y polarization preference (or vice versa). It is interesting to

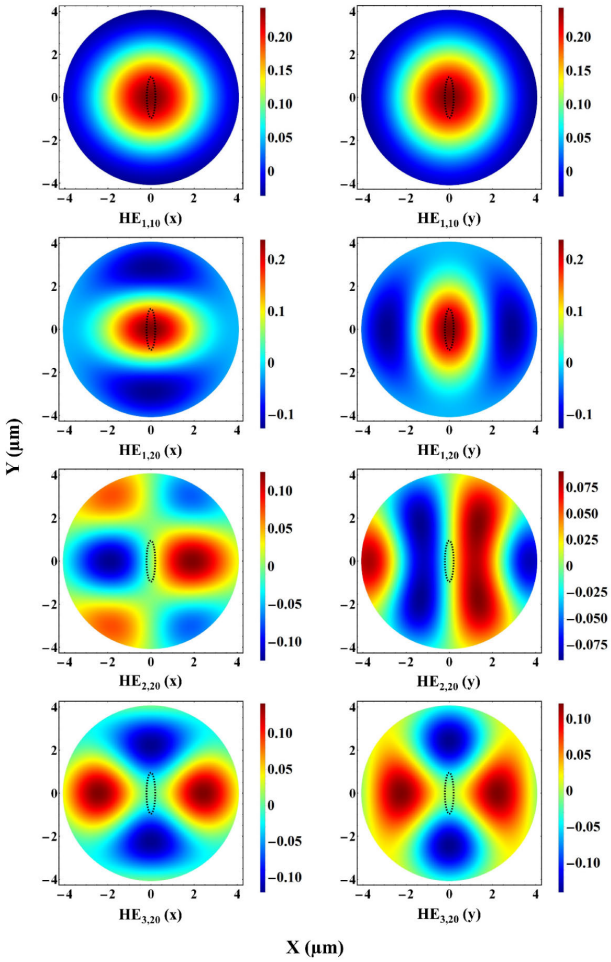

FIGURE 3. Exemplary overlap fields between core mode and $HE_{l,m}$ cladding modes for x and y polarizations in the core region. The ellipse in each figure indicates the RIM region, corresponding to the area of integration for the calculation of coupling coefficients. Strong coupling is expected when the RIM occupies more area with the same and deep color (e.g. deep red for $HE_{1,10}$ mode), whereas contribution from positive (red) and negative (blue) can cancel out (as represented by $HE_{2,20}$ mode), resulting in weak or even zero coupling strength.

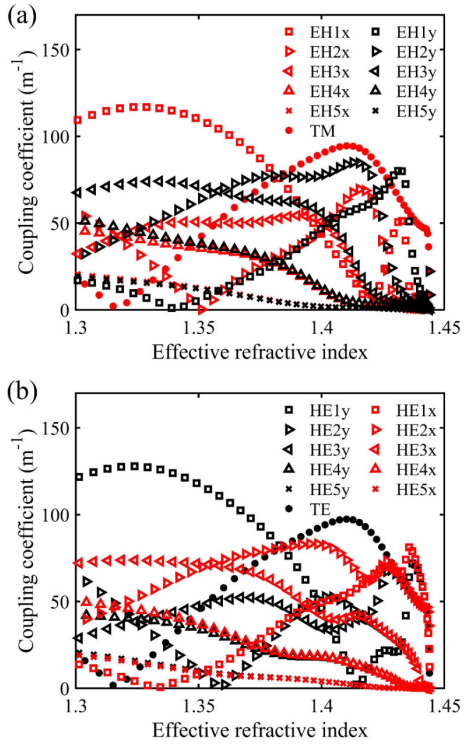

FIGURE 4. Coupling coefficients of cladding modes with AO up to 5 in ELFBG. X and y indicate the polarization along x and y axis, and are represented by red and black color, respectively.

note that, in the ERI range indicated by blue shadow, $HE_{1,m}$ modes prefer coupling from y polarization, whereas $HE_{2,m}$ modes prefer coupling from x polarization. Such opposite polarization preference is quite different from that of TFBGs, where HE/TE (EH/TM) modes have the same polarization preference [1], [24].

To understand the polarization dependent coupling behaviors of ELFBG, Fig. 6 depicts several representative overlap fields of $HE_{1,m}$ modes and $HE_{2,m}$ modes. The polarization dependence of low RO modes has been illustrated by $HE_{1,10}$ cladding mode in Fig. 3, which is weak even with eccentric RIM. For other modes, as represented by $HE_{1,20}$ and $HE_{2,40}$ modes in Fig. 6, the reason for the polarization dependence is similar: with the increase of mode RO, additional overlap ring with opposite sign enters into the core region, and when the RIM locates around the position where the overlap field transits its sign, e.g., from positive to negative [$HE_{1,20}$ (y) and $HE_{2,40}$ (y) in Fig. 6], the negative and positive contributions cancel out and the corresponding coupling is suppressed. Therefore, coupling from x polarization is preferred for those modes. The polarization dependence of $HE_{1,m}$ modes switches with further increase of mode RO (after the position indicated by green arrow in Fig. 5), as shown by the overlap field of $HE_{1,40}$ mode in Fig. 6, where another overlap ring falls into the core region. In this way, the cancellation occurs between the innermost three rings for x polarization, whereas the RIM now locates at area with strong interaction for y polarization. As a result, coupling preference is switched from x polarization to y polarization.

B. TRANSMISSION SPECTRA

The polarization dependences differ between modes with different AO, and as too many modes are involved, their combined effects on the grating cannot be observed directly from coupling coefficients, and will be detailed this section with the calculated transmission spectra. Fig. 7 depicts the transmission spectra of CLFBG and ELFBG for x and y input polarizations, and the resonant wavelengths of $EH/HE_{1,m}$ and $EH/HE_{2,m}$ modes determined by phase matching condition are also shown. The resonant wavelengths of cladding modes with higher AO are not depicted in Fig. 7b because they are approximately the same for even (odd) AO cladding modes and thus, can be represented by that of $EH/HE_{2,m}$ ($EH/HE_{1,m}$) modes [13]. Comparing Fig. 7a with Fig. 7c, we can see that the spectra of ELFBG exhibit a denser comb, because in ELFBG, additional resonances are generated from coupling

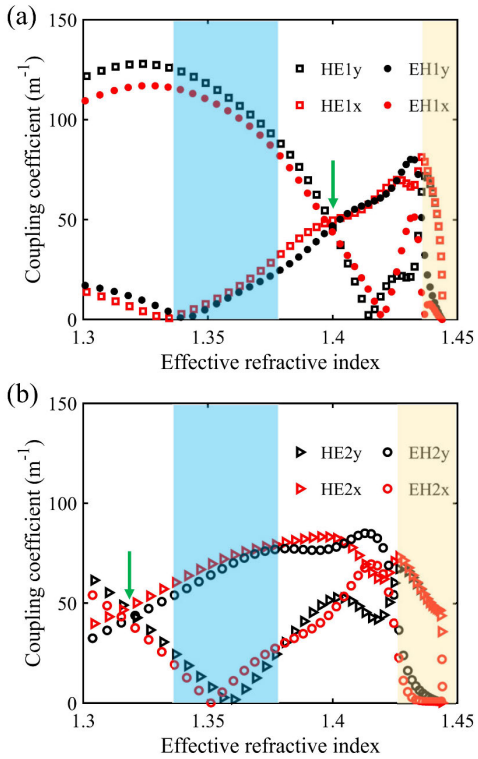

FIGURE 5. Coupling coefficients of $HE_{1,m}$ and $HE_{2,m}$ modes in ELFBG for x and y polarizations. For each set of modes (e.g. $HE_{1,m}$), the coupling coefficients are almost the same for both polarizations in the yellow area, suggesting weak polarization dependence, whereas in the blue area, strong polarization dependence is presented. The green arrows indicate the position where the polarization preference switches, i.e., from x polarization preference to y polarization preference (or vice versa).

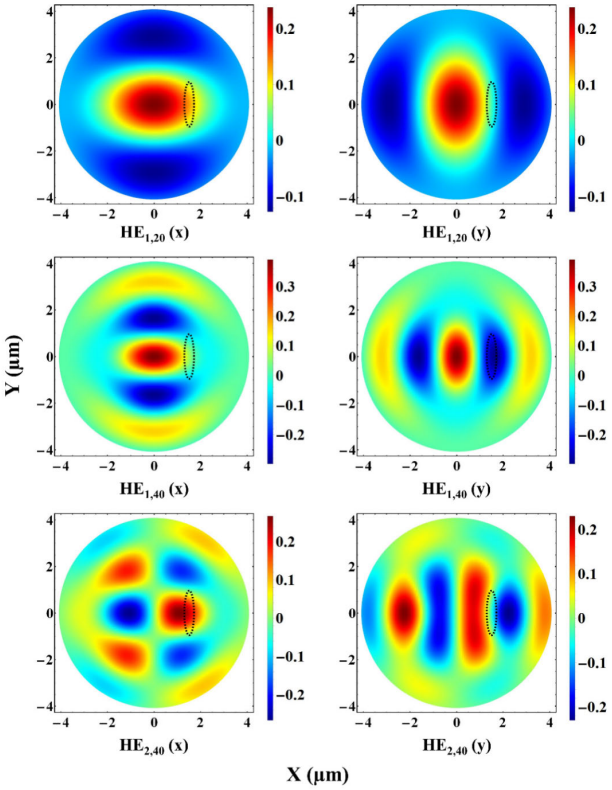

FIGURE 6. Exemplary overlap fields between core mode and $HE_{l,m}$ cladding modes for x and y polarizations in the core region. The ellipse in each figure indicates the RIM region, corresponding to the area of integration for the calculation of coupling coefficients. Due to the cancellation of negative (blue) and positive (red) contributions, $HE_{1,20}$ and $HE_{2,40}$ mode exhibit x polarization preference, and $HE_{1,40}$ mode exhibit y polarization preference.

to cladding modes with even AO, which appear alternatively with odd AO mode resonances (Fig. 7b). It can be seen from Fig. 7b that, due to the quasi-degeneracy of EH/HE modes, their resonant wavelengths appear in pair [24], [25].

In terms of polarization dependence, for CLFBG, the spectra of the two polarization differ in strength only, whereas no additional resonances appear for different polarizations. This is expectable from their coupling coefficients detailed in last section. A much stronger polarization dependence can be observed from the spectra of ELFBG. The polarization dependence varies with increased wavelength separation from core mode resonances at the longest wavelength (corresponding to cladding modes with increased RO). According to the polarization dependent spectral features, we divide the spectra into four wavelength ranges, with more details depicted in Fig. 7(d-g):

- Single peaks in Fig. 7d, with stronger polarization dependence for even AO mode resonances (denoted by blue dotted rectangles) than odd AO mode resonances. The polarization dependence of hybrid modes is weak, as represented by $HE_{1,10}$ mode in Fig. 3, which has circularly quasi-symmetric overlap field within the core. The relatively stronger polarization dependence for even AO mode resonances mainly results from the strong polarization dependent coupling to TE/TM modes, which are degenerate with even AO hybrid modes;

- Single peaks with opposite strong polarization dependence for neighboring resonances in Fig. 7e, due to the fact that they are generated from coupling to cladding modes with even and odd AO, which have opposite polarization dependence, as represented by $HE/EH_{1,m}$ and $HE/EH_{2,m}$ modes in Fig. 5. Such polarization dependence is different from that of TFBG, which shows the same polarization dependence for both even and odd AO cladding modes [1], [24], and can be experimentally verified with previous reports (inset of Fig. 2 in [15]).

- Alternative single- and dual- peaks in Fig. 7f. In this wavelength range, cladding modes with even AO exhibit decreased polarization preference, thus generating dual peaks for each polarization, whereas stronger polarization preference is maintained for odd AO modes.

- Dual peaks in Fig. 7g, where the polarization dependence remains, but becomes much weaker, and dual peaks with polarization dependent strength are generated. This confirms with the transition from single- to dual- peaks in experimental reports [15].

In the previous analyses, we only consider the polarization dependence generated from mode structure and RIM position. To further verify out analyses, the birefringence induced by eccentric inscription is taken into account.

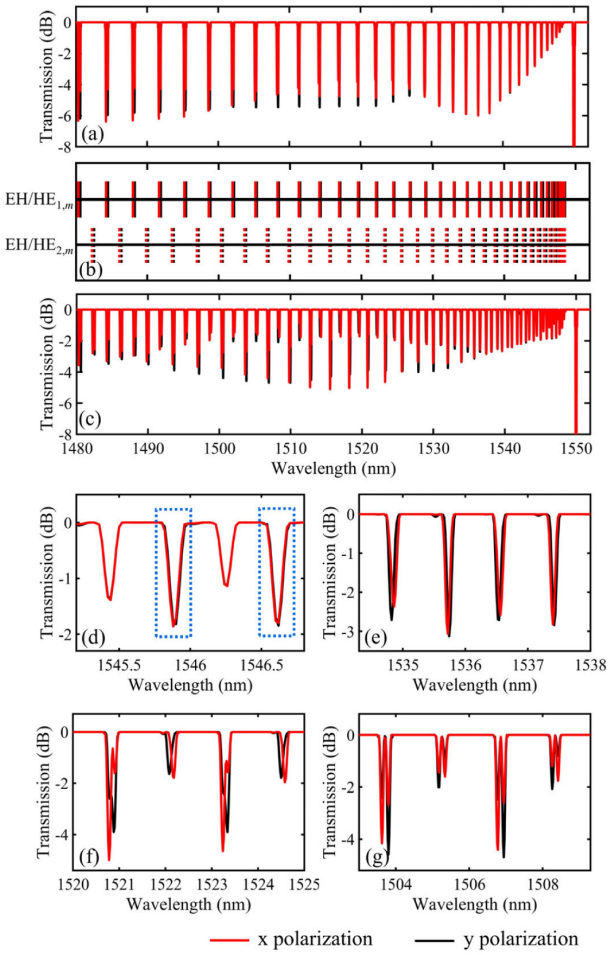

FIGURE 7. (a) Transmission spectra of CLFBG, (b) resonant wavelengths of $EH/HE_{1,m}$ and $EH/HE_{2,m}$ modes calculated from the phase matching condition, (c) transmission spectra of ELFBG with a offset of 1.5 μm along x axis, and typical spectra of ELFBG with more details in (d) single peaks with stronger polarization dependence for even AO mode resonances (denoted by blue dotted rectangles) than odd AO mode resonances, (e) single peaks with opposite strong polarization dependence for neighboring resonances, (f) alternative single- and dual- peaks, and (g) dual peaks. Red and black lines indicate spectra of x and y polarizations respectively.

As the RIM has a transverse dimension less than 2 μm, which is much smaller than the fiber cladding (125 μm diameter), we can assume that such birefringence exists for core mode only. According to the phase matching condition [(1)], the wavelength separation of cladding modes resonances induced by this birefringence can be determined as:

$$\Delta\lambda_{cl} = \lambda_{cl,x} - \lambda_{cl,y} = (neff_x^{co} - neff_y^{co}) \cdot \Lambda \qquad (3)$$

where Λ is the grating period, and $neff_x^{co}$ and $neff_y^{co}$ are the ERI of x and y polarized core mode respectively. With the experimentally measured birefringence of 1.05×10^{-4} [15], the induced wavelength separation between two polarizations is ~56.5 pm for cladding mode resonances. Taking this into account, as shown in Fig. 8, a better agreement can be achieved with existed experimental report [15], where the matched wavelength between two polarization (indicated by green arrow in Fig. 8) can be numerically reproduced.

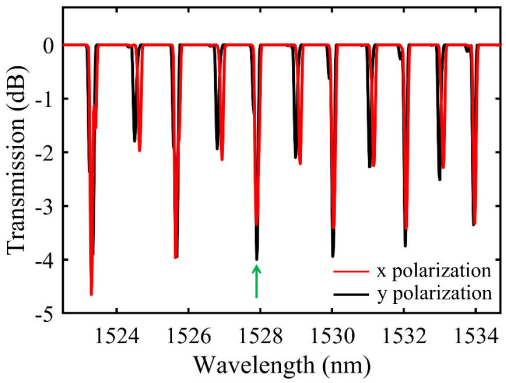

FIGURE 8. Transmission spectra of ELFBG considering inscription induced birefringence. Red and black lines represent x and y polarizations respectively. The green arrow indicates the matched wavelength between two polarizations.

C. THE EFFECT OF ECCENTRIC DIRECTION

The above discussion has been limited to eccentricity along x axis. For eccentricity along y axis (see Fig. 9a), if we define a new coordinate (x', y'), as depicted by Fig. 9b, and rotate Fig. 9b by 90 degree in the clockwise direction, we can get Fig. 9c. In this way, the eccentricity along y axis can be transformed into eccentricity along x' axis, with reversed width and height of the RIM. Therefore, with the reversed dimension of RIM taken into consideration, the principles discussed above is applicable to this case.

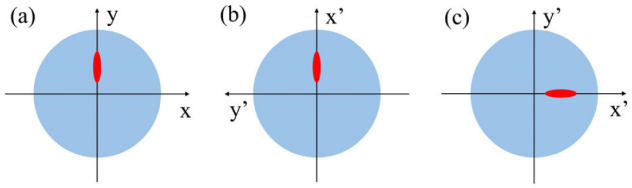

FIGURE 9. Schematic of (a) RIM with eccentricity along y axis, (b) RIM under newly defined coordinate (x', y'), and (c) rotation of (b) by 90 degree in the clockwise direction.

IV. CONCLUSION

In conclusion, we have numerically investigated the cladding mode coupling characteristics of LFBG, focusing on the polarization dependence in ELFBG. Both CLFBG and ELFBG allow strong coupling to cladding modes, resulting in comb-like spectra similar to but not the same as that of TFBGs, which are analyzed in detail.

For CLFBG, coupling to $EH/EH_{1,m}$ cladding modes dominates, with a little coupling to $EH/EH_{3,m}$ cladding modes, whereas coupling to cladding modes with even AO is fully suppressed due to their mode symmetry. Such coupling presents weak polarization dependence, as can be observed from the calculated coupling coefficient and spectra of both polarizations.

For ELFBG, which is more of our concern, strong polarization dependence exists. Such polarization dependence mainly results from the mode structure that varies with mode order,

and at certain mode order, coupling from one polarization is cancelled out, resulting in a polarization selective coupling. The polarization dependence coupling can be seen more clearly in the transmission spectra, which features four types of resonance peaks. Note that cladding mode resonances with opposite polarization dependence can be observed. This is unique in eccentric grating and can be explained by the fact that even and odd AO modes cancel out in a different manner and therefore, presents a different polarization dependence. Our numerical results agree well with previous experimental reports, and a better agreement can be achieved by further considering the birefringence induced by grating inscription. Our analyses can help understand the working principles of LFBG and facilitate their applications, especially the polarization assisted sensing such as those based on SPR.

REFERENCES

[1] J. Albert, L.-Y. Shao, and C. Caucheteur, "Tilted fiber Bragg grating sensors," *Laser Photon. Rev.*, vol. 7, no. 1, pp. 83–108, Feb. 2012.

[2] W. Zhou, Y. Zhou, and J. Albert, "A true fiber optic refractometer," *Laser Photon. Rev.*, vol. 11, no. 1, Jan. 2017, Art. no. 1600157.

[3] C. F. Chan, C. Chen, A. Jafari, A. Laronche, D. J. Thomson, and J. Albert, "Optical fiber refractometer using narrowband cladding-mode resonance shifts," *Appl. Opt.*, vol. 46, no. 7, pp. 1142–1149, Mar. 2017.

[4] T. Guo, F. Liu, B.-O. Guan, and J. Albert, "[INVITED] Tilted fiber grating mechanical and biochemical sensors," *Opt. Laser Technol.*, vol. 78, pp. 19–33, Apr. 2016.

[5] F. Chiavaioli, F. Baldini, S. Tombelli, C. Trono, and A. Giannetti, "Biosensing with optical fiber gratings," *Nanophotonics*, vol. 6, no. 4, pp. 663–679, Jun. 2017.

[6] B. Jiang, X. Lu, X. Gan, M. Qi, Y. Wang, L. Han, D. Mao, W. Zhang, Z. Ren, and J. Zhao, "Graphene-coated tilted fiber-Bragg grating for enhanced sensing in low-refractive-index region," *Opt. Lett.*, vol. 40, no. 17, pp. 3994–3997, Sep. 2015.

[7] C. Caucheteur, Y. Shevchenko, L.-Y. Shao, M. Wuilpart, and J. Albert, "High resolution interrogation of tilted fiber grating SPR sensors from polarization properties measurement," *Opt. Exp.*, vol. 19, no. 2, pp. 1656–1664, 2011.

[8] K. Chah, V. Voisin, D. Kinet, and C. Caucheteur, "Surface plasmon resonance in eccentric femtosecond-laser-induced fiber Bragg gratings," *Opt. Lett.*, vol. 39, no. 24, pp. 6887–6890, Dec. 2014.

[9] H. Chikh-Bled, M. Debbal, M. Chikh-Bled, C. Ouadah, V. Calero-Vila, and M. Bouregaa, "Refractive index sensor in eccentric fiber Bragg gratings using a point-by-point IR femtosecond laser," *Appl. Opt.*, vol. 58, no. 3, pp. 528–534, Jan. 2019.

[10] A. Martinez, M. Dubov, I. Khrushchev, and I. Bennion, "Direct writing of fibre Bragg gratings by femtosecond laser," *Electron. Lett.*, vol. 40, no. 19, pp. 1170–1172, Sep. 2004.

[11] A. Martinez, M. Dubov, I. Khrushchev, and I. Bennion, "Photoinduced modifications in fiber gratings inscribed directly by infrared femtosecond irradiation," *IEEE Photon. Technol. Lett.*, vol. 18, no. 21, pp. 2266–2268, Nov. 2006.

[12] Y. Lai, K. Zhou, K. Sugden, and I. Bennion, "Point-by-point inscription of first-order fiber Bragg grating for C-band applications," *Opt. Exp.*, vol. 15, no. 26, pp. 18318–18325, Dec. 2007.

[13] J. Thomas, N. Jovanovic, R. G. Becker, and G. Marshall, "Cladding mode coupling in highly localized fiber Bragg gratings: Modal properties and transmission spectra," *Opt. Exp.*, vol. 19, no. 1, pp. 325–341, Dec. 2010.

[14] J. U. Thomas, N. Jovanovic, and R. G. Krämer, "Cladding mode coupling in highly localized fiber Bragg gratings II: Complete vectorial analysis," *Opt. Exp.*, vol. 20, no. 19, pp. 21434–21449, Sep. 2012.

[15] H. Chikh-Bled, K. Chah, Á. González-Vila, B. Lasri, and C. Caucheteur, "Behavior of femtosecond laser-induced eccentric fiber Bragg gratings at very high temperatures," *Opt. Lett.*, vol. 41, no. 17, pp. 4048–4051, Sep. 2016.

[16] C. Caucheteur, T. Guo, and J. Albert, "Polarization-assisted fiber Bragg grating sensors: Tutorial and review," *J. Lightw. Technol.*, vol. 35, no. 16, pp. 3311–3322, Aug. 15, 2017.

[17] Y.-C. Lu, R. Geng, C. Wang, F. Zhang, C. Liu, T. Ning, and S. Jian, "Polarization effects in tilted fiber Bragg grating refractometers," *J. Lightw. Technol.*, vol. 28, no. 11, pp. 1677–1684, Jun. 2010.

[18] Z. Li, Z. Yu, Y. Shen, X. Ruan, and Y. Dai, "Graphene enhanced leaky mode resonance in tilted fiber Bragg grating: A new opportunity for highly sensitive fiber optic sensor," *IEEE Access*, vol. 7, pp. 26641–26651, 2019.

[19] C. Tsao, D. Payne, and W. A. Gambling, "Modal characteristics of three-layered optical fiber waveguides: A modified approach," *J. Opt. Soc. Amer. A, Opt. Image Sci.*, vol. 6, np. 4, pp. 555–563, Apr. 1989.

[20] T. Erdogan, "Fiber grating spectra," *J. Lightw. Technol.*, vol. 15, no. 8, pp. 1277–1294, Aug. 1997.

[21] T. Erdogan, "Cladding-mode resonances in short-and long-period fiber grating filters," *J. Opt. Soc. Amer. A, Opt. Image Sci.*, vol. 14, no. 8, pp. 1760–1773, Nov. 1997.

[22] J. Thomas, C. Voigtländer, S. Nolte, A. Tünnermann, N. Jovanovic, G. D. Marshall, M. J. Withford, and M. Steel, "Mode selective fiber Bragg gratings," in *Proc. SPIE Frontiers Ultrafast Opt., Biomed., Sci., Ind. Appl.*, vol. 7589, Feb. 2010, Art. no. 75890J.

[23] P. Lu, D. Grobnic, and S. J. Mihailov, "Characterization of the birefringence in fiber Bragg gratings fabricated with an ultrafast-infrared laser," *J. Lightw. Technol.*, vol. 25, no. 3, pp. 779–786, Mar. 2007.

[24] M. Z. Alam and J. Albert, "Selective excitation of radially and azimuthally polarized optical fiber cladding modes," *J. Lightw. Technol.*, vol. 31, no. 19, pp. 3167–3175, Oct. 2013.

[25] F. Shen, K. Zhou, C. Wang, H. Jiang, D. Peng, H. Xia, K. Xie, and L. Zhang, "Polarization dependent cladding modes coupling and spectral analyses of excessively tilted fiber grating," *Opt. Exp.*, vol. 28, no. 2, pp. 1076–1083, Jan. 2020.

FANGCHENG SHEN was born in Anhui, China, in 1993. He received the B.S. degree in opto-electronic information engineering and the Ph.D. degree in optical engineering from the Huazhong University of Science and Technology, China, in 2013 and 2018, respectively. He is currently a Lecturer with the Guangdong University of Technology, China. His current research interests include fiber optic sensor and fiber optic devices.

TINGTING ZHANG was born in Jiangsu, China, in 1990. She received the B.S. degree in material physics and the M.S. degree in optical engineering from Nanjing University, China, in 2008 and 2015, respectively, and the Ph.D. degree in optical engineering from Aston University, U.K., in 2020. Her current research interests include fiber optic communication and fiber optical devices.